Design and Testing of an Autorotative Payload Delivery System



Anne Brindejonc
Graduate Research Assistant

Jayant Sirohi*
Assistant Research Scientist

Inderjit Chopra
Alfred Gessow Professor and Director

Alfred Gessow Rotorcraft Center, Department of Aerospace Engineering
University of Maryland, College Park, MD

The design, testing, and analysis of an autonomous autorotative payload delivery system called the Autobody is presented. The Autobody must be capable of passively deploying a payload from a conventional aircraft, by means of an autorotative rotor. Operational requirements specify the Autobody to have a four bladed rotor with a diameter of four feet, a total mass of 2.27 kg (5 lb) and a maximum steady state descent velocity of 4.57 m/s (15 ft/s). A novel rotor hub design incorporating negative pitch–flap coupling in conjunction with negative blade pitch and a negative precone is implemented to passively achieve the transition to steady autorotation. An analysis is developed to predict the steady state behavior of the Autobody. Only vertical autorotation is considered as it will result in a conservative design and is the simplest state to analyze. Wind tunnel tests were performed on a scaled model rotor to validate the analysis and to investigate the effect of different rotor parameters. The analysis was then used to perform a parametric study of the effect of several rotor variables on the system performance, from which an optimum full scale configuration is identified. An instrumented full scale prototype was flight tested by dropping it from a hot air balloon. For an Autobody of mass 2.27 kg, with a -41° pitch-flap coupling angle, a -10° fixed collective pitch, and a -4° precone, a steady state descent velocity of 4.11 m/s (13.5 ft/s) was observed. Based on the predictions and the flight tests, it was concluded that the proposed Autobody design satisfactorily meets all operational requirements.

Nomenclature

a_o^a	coefficient of thrust predicted by analysis
a_o^e	coefficient of measured thrust
b^a	coefficient of rotational speed predicted by analysis
b^e	coefficient of measured rotational speed
C_d	drag coefficient
C_l	lift coefficient
C_{l_α}	lift curve slope
C_Q	torque coefficient
C_T	thrust coefficient
dD	elemental drag force
dF_z	vertical force at blade element
dL	elemental lift force
dQ	torque on annular element
dr	width of annular element
dT	thrust on annular element
E_T	error between measured and predicted thrust
E_{RPM}	error between measured and predicted rotational speed
F	resultant force
I_b	blade flapping inertia
k_β	blade flapping stiffness
$\bar{M}_{\text{AF}}$	total nondimensional aerodynamic flapping moment
m_b	blade mass
Q	rotor torque
r	radial location
T	rotor thrust
T_{ana}	predicted thrust
T_{exp}	measured thrust
u_T	velocity in-plane of rotor disk
u_p	velocity out-of-plane of rotor disk
V_d	descent velocity
v_h	induced velocity in hover
α	angle of attack
β	flapping angle
β_p	precone angle
δ_3	angle of flapping hinge (pitch-flap coupling angle)
$\Delta\beta$	change in flapping angle
$\Delta\theta$	change in blade pitch angle
θ	blade pitch angle
θ_o	blade root pitch angle
θ_{TW}	blade twist rate
λ	induced velocity ratio
λ_d	descent velocity ratio
ν_{β_o}	nonrotating flapping frequency
ν_{β_e}	rotating flapping frequency
σ	blade solidity
Ω	rotor rotational speed
Ω_{ana}	predicted rotational speed
Ω_{exp}	measured rotational speed

*Corresponding author; email: sirohij@umd.edu.

Presented, in part, at the 61st Annual Forum of the American Helicopter Society International, Grapevine, TX, June 1–3, 2005. Manuscript received August 2006; accepted July 2007.

Introduction

Autonomous unmanned aerial vehicles (UAVs) find numerous applications in hazardous civilian and military environments, which include aerial reconnaissance and surveillance of enemy territory, traffic

monitoring, and search and rescue operations. Recently, there has been considerable interest in the design and development of versatile, cost-effective, autonomous UAVs, which are capable of deploying electronic instruments on ground from conventional aircraft. Such a vehicle is required to decelerate the payload to a low descent velocity in order to minimize the impact load on the sensitive onboard electronic equipment. A delivery system called the Autobody is envisaged to safely deploy a payload dropped from an aircraft. The main feature of the Autobody is an autorotative rotor to produce lift, thus eliminating the need for an on-board engine. An autorotative rotor was preferred over other decelerating devices, such as a parachute, for several reasons (Ref. 1). For example, an autorotative system eliminates the sudden deceleration during deployment, smoothing out the descent. In addition, once deployed, power can be provided to the on-board instrumentation with solar cells embedded in the rotor blades.

The objective of the present study is to design a passively controlled, autorotative rotor with minimum mechanical complexity and minimum weight penalty. The vehicle must satisfy certain operational constraints imposed by the specific deployment scenario. These include a maximum gross weight of 2.27 kg (5 lb), a four bladed rotor of 1.22 m (4 ft) diameter, and a maximum steady state rate of descent of 4.57 m/s (15 ft/s). It is known that the minimum rate of descent occurs for autorotation with some forward velocity, hence designing the rotor for the specified maximum rate of descent in vertical autorotation results in a conservative design. In addition, vertical autorotation presents the simplest case for analysis. Therefore, the present study only considers purely vertical autorotation.

Several authors have discussed the phenomenon of steady autorotation (Refs. 2–5). Because momentum theory is not valid in this rotor operating condition, semi-empirical models are typically used for analysis. Although steady autorotation is well documented and understood, there is little data on rotors starting from rest and experiencing a transient state before reaching autorotation.

The concept of an autorotative vehicle dropped from an aircraft has been previously explored by some researchers. During the second world war, Hafner developed a manned autogyro glider, the Rotachute, capable of delivering a human payload from a large transport aircraft (Ref. 6), and a larger system named the Rotabuggy. In 1942, Flugzeugwerke developed the Fa-33 (Ref. 6), which was an autogyro towed behind a submarine for surveillance purposes. In 2003, Bartz and Miklosovic (Ref. 7) investigated the effect of airfoil camber on the autorotation and deceleration performance of an Autorotor. However, the Autorotor was equipped with a controllable outboard flap.

The idea of an autorotative rotor mounted on a spacecraft to lower its rate of descent during re-entry has also been widely investigated. Wernicke (Ref. 8) presented a preliminary experimental study of a model Spacecraft Rotor Landing System. Kretz (Ref. 9) developed a rotor-based re-entry system, called the Space Rotor, that incorporated actively controlled blade collective pitch. Levin and Smith (Refs. 10, 11) performed wind tunnel tests on a rotor/launcher assembly to determine the achievable performance gains. The Roton, developed by the Rotary Rocket Company (Ref. 1), was capable of taking off vertically like a rocket under the control of a crew, delivering a 3,175-kg (7,000 lb) payload to low earth orbit, and slowing down during re-entry by means of an autorotative rotor.

These concepts, while being innovative, were actively controlled. Conventional piloted helicopters enter into autorotation in case of engine failure. A key function of the pilot during autorotation is to ensure that the rotor speed does not decrease below a certain acceptable value. Flying in this state requires constant pilot inputs to control the blade pitch and therefore the rate of descent. In the case of the Autobody, the rotor starts from rest, and must transition to steady autorotation.

A theoretical study of the feasibility of a fully autonomous, autorotative system with no on-board active control systems was performed by Sirohi et al. (Ref. 12). This study proposed a rotor with a negative precone and a negative pitch-flap coupling to achieve the required change in collective pitch in flight. The rotor started from rest and underwent a transient state before reaching steady autorotation. While the basic concepts were discussed and a parametric study performed, the theoretical analysis needed to be refined and validated with wind tunnel data and flight test data. The present study complements this work.

The present paper describes the design of an autorotative rotor with completely passive operation. The development of the theory to predict the steady state behavior of the system is presented. The analysis was validated with wind tunnel tests performed on a quarter scale model. The validated analysis was used to carry out a parametric study to minimize the rate of descent of the Autobody. A full scale prototype was fabricated and flight tested by dropping it from a hot air balloon. This represents vertical autorotation, and ignores any effects of forward wind velocity that the Autobody might encounter while being deployed from an aircraft. Data measured during the flight test is used to further validate the analysis.

Physical Principles

The rotor of the Autobody starts from rest, and the rotor rotation needs to be initiated in the correct direction. As the system descends, the rotor spins up and has to produce an increasing thrust. In the steady state, the thrust must be equal to the total weight of the system. The descent velocity should be as low as possible to permit a safe landing. This can be achieved by maximizing the rotor thrust for a given descent velocity.

The resultant force F acting on a rotor blade as it starts from rest is shown in Fig. 1. Just after the vehicle is released, the rotor rotational speed (RPM) and the in-plane velocity of the blades, u_T are both equal to zero. An out-of-plane velocity, u_p is present, and is equal and opposite to V_d, the descending velocity of the system. If the blade is set at a positive pitch, the resultant force F will have an in-plane component acting towards the trailing edge. This causes the rotor to start rotating trailing edge first. If the blade is set at a negative pitch, the in-plane force causes the rotor to spin up in the correct direction: leading edge first. However, a low value of blade pitch results in a low steady state thrust. Therefore, to obtain a high steady state thrust, a passive increase in pitch is needed as the RPM increases. To achieve this, a negative δ_3 angle is incorporated at the blade flap hinge, yielding a negative pitch-flap coupling. As a result, an increase in flap angle will result in an increase in blade pitch. The relationship between blade pitch and flap angle is expressed as

$$\begin{aligned}\Delta\theta &= -\Delta\beta\tan(\delta_3)\\ &= -(\beta-\beta_p)\tan(\delta_3)\end{aligned} \tag{1}$$

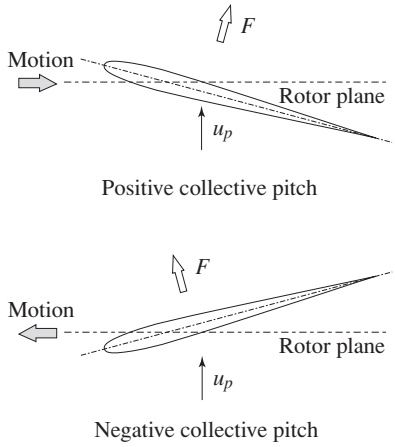

Fig. 1. Effect of blade collective pitch on the direction of rotation.

where $\Delta\theta$ is the change in pitch angle, $\Delta\beta$ the change in flap angle, and β_p is the blade precone angle. Note that if $\beta_p < 0$, then $\Delta\theta$ is greater than it would be if $\beta_p > 0$. In other words, introducing a negative precone angle further increases the blade pitch.

Based on these observations, the final hub design incorporates the following features: 1) a negative blade pitch angle θ_o to initiate rotation in the correct direction, 2) a negative precone angle β_p to allow a large change in flap deflection, and 3) a negative δ_3 angle to convert the change in flap deflection to an increase of blade pitch. While descending, the rotor speeds up leading to an increase in lift and centrifugal force on each blade. As a result, the blade flaps up, which because of the δ_3 coupling, results in an increase in blade pitch. This causes a further increase in the lift and torque on the rotor. The rotor RPM increases continuously until the equilibrium condition is arrived: a constant RPM and a zero net rotor torque. In this manner, a passive increase in the rotor collective pitch, and a transition to a state of steady autorotation is achieved.

Analytical Model: The RPM Sweep Method

The aim of the analysis, called the RPM sweep method, is to predict the rotor thrust and RPM when it has reached the steady state of autorotation. The analysis is validated with experiments performed on a scaled model rotor in an open-jet wind tunnel, and is then used to design a full scale prototype. Note that typical estimates of autorotative rates of descent for helicopters rely on empirical data (Refs. 2, 4), and some researchers have experimented with powered rotor models in wind tunnels in order to improve the understanding of these empirical relations (Ref. 13). The goal of the present analysis is to design an optimum rotor geometry to minimize the descent velocity of the Autobody.

For a given descent velocity V_d, a value of rotor RPM is chosen for which the rotor thrust T and torque Q are calculated from blade element momentum theory (BEMT). The chosen RPM starts from a value that represents a large negative ratio of descent velocity to hover induced velocity (ratio V_d/v_h) and gradually increases until it approaches the ratio $V_d/v_h = -2$. In this way, the chosen RPMs sweep through the windmill brake state of the rotor. Calculation is stopped if $V_d/v_h \geq -2$, beyond which momentum theory is not valid. The calculated rotor torque coefficients are plotted versus RPM and the curve is extrapolated to find the point of zero rotor torque (Fig. 2). This point corresponds to steady state autorotation. The rotor thrust and torque are calculated based on the RPM at this point.

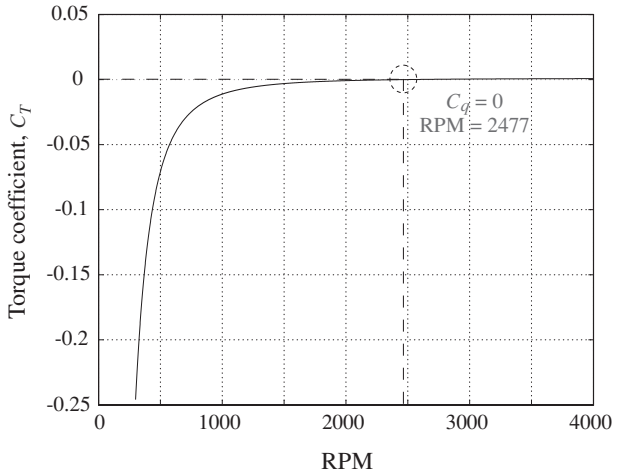

Fig. 2. Sample result of rotor torque coefficient versus RPM given by the RPM sweep method.

The RPM sweep analysis assumes purely axial flow and sea level conditions. The blades are assumed rigid and undergo flap and pitch degrees of freedom. The analysis includes blade dynamics and kinematic pitch-flap coupling in conjunction with an asymptotic solution procedure based on a refined blade element theory. The lift coefficient at each blade element is determined by $C_l = C_{l\alpha}\alpha$, where $C_{l\alpha} = 5.73$ /rad is the lift curve slope, and α is the angle of attack. The drag coefficient at each blade element is taken to be constant, $C_d = 0.04$. This value is slightly higher than the typical value as the rotor blades are in a low Reynolds number environment. Given a descent velocity and a rotational velocity, the inflow, aerodynamic angles and elemental forces are computed at each blade element until the blade flap angle converges. The integrated values of rotor thrust and torque are then determined. The basic algorithm is as follows:

1) Step 1: Inputs and initial conditions. Input data include the assumed RPM, rotor parameters (including blade pitch, precone and pitch-flap coupling), and descent velocity.

2) Step 2: Calculation of inflow. The inflow λ at a rotor annulus of width dr at a radial station r, is calculated by the blade element momentum theory as

$$\lambda = -\frac{\lambda_d}{2} + \frac{\sigma C_{l\alpha}}{16} + \sqrt{\left(\frac{\lambda_d}{2} - \frac{\sigma C_{l\alpha}}{16}\right)^2 - \frac{\sigma C_{l\alpha}\theta r}{8}} \tag{2}$$

where σ is the rotor solidity, θ is the pitch angle and λ_d is the descent velocity ratio.

3) Step 3: Calculation of aerodynamic angles and elemental forces. Based on the inflow calculated in Step 2, and the pitch angle at each blade element, the aerodynamic angles are calculated. The spanwise pitch angle is given by

$$\theta(r) = \theta_o + r\theta_{\mathrm{TW}} + \Delta\theta \tag{3}$$

where θ_o is the blade root pitch, θ_{TW} is the twist rate and $\Delta\theta$ is the change of pitch, written as

$$\begin{aligned}\Delta\theta &= -\tan(\delta_3)\Delta\beta \\ &= -\tan(\delta_3)(\beta - \beta_p)\end{aligned} \tag{4}$$

The change in flap angle, $\Delta\beta$, is initially equal to zero. The elemental lift dL and drag dD as well as the components of the elemental forces along the horizontal and vertical axes are calculated at each blade segment. The elemental thrust dT and torque dQ are then computed on each annulus.

The total nondimensional aerodynamic flapping moment on the blade, $\bar{M}_{\mathrm{AF}}$, is

$$\bar{M}_{\mathrm{AF}} = \frac{\int_0^R dF_z}{\Omega^2 I_b} \tag{5}$$

where dF_z is the vertical force at the blade element and I_b is the moment of inertia of the blade about the flapping hinge. The steady flap angle β is calculated from the steady state flapping equation as

$$\beta = \frac{\bar{M}_{\mathrm{AF}}}{\nu_{\beta_e}^2} + \beta_p \frac{\nu_{\beta_o}^2}{\nu_{\beta_e}^2} \tag{6}$$

where the nonrotating flapping frequency ν_{β_o} and rotating flapping frequency ν_{β_e} are defined as

$$\nu_{\beta_o} = \sqrt{\frac{k_\beta}{I_b\,\Omega^2}} \tag{7}$$

$$\nu_{\beta_e} = \sqrt{\nu_{\beta_o}^2 + 1} \tag{8}$$

The change in pitch angle is then obtained using Eq. (4), and several iterations are performed until β converges. The total rotor thrust T, torque Q, thrust coefficient C_T and torque coefficient C_Q are then calculated.

4) Step 4: Check rotor operating regime. If $-2 < V_d/v_h < 0$, momentum theory is no longer valid, and the calculation is stopped. The curve of C_Q versus RPM is extrapolated to find the RPM at which $C_Q = 0$. If $V_d/v_h < -2$, then the computation proceeds to the next RPM.

Wind Tunnel Tests

The performance of a scaled model of the rotor was evaluated by mounting it in an open jet wind tunnel such that the wind flowed through the rotor in a condition of axial descent. The main goal of the wind tunnel tests was to validate the RPM sweep method. Steady RPM and thrust were measured for different sets of rotor parameters. Because the wind tunnel offered a controlled environment, the influence of blade pitch and precone and pitch-flap coupling on the steady state could be investigated.

Model rotor construction

A scaled model rotor of diameter 0.33 m (13 inches) was sized to fit the dimensions of the test section (0.533 m (21 inches) × 0.533 m (21 inches)) of an open-jet wind tunnel. The characteristics of the model rotor are shown in Table 1 and the main features of the rotor are shown in Fig. 3. Note that while the figures show a four-bladed rotor, the final wind tunnel tests were performed with a two-bladed rotor in order to minimize errors inherent in manually setting the blade pitch. The model blade grips feature a flexure based flap hinge with a δ_3 angle machined at -30° or -50° (Fig. 4). As a result of the finite width of the flexure, it was found that the effective flap hinge line was not along the machined hinge axis. The actual δ_3 angles were measured to be -29.74° for the -50° case and -17.33° for the -30° case. Grips without δ_3 were also manufactured to test the case of no pitch-flap coupling. The hub features a negative precone of $\beta_p = 0^\circ$, $\beta_p = -4^\circ$ or $\beta_p = -6^\circ$. A negative blade pitch can be set (Fig. 3) by rotating the grip around the hub fixture. The blades are made of 31-Rohacell foam, of density 32 kg/m^3, and covered with one ply of carbon fiber prepeg.

Wind tunnel test setup

Autorotation was simulated by a free-spinning hub (the torque on hub is zero at steady state) and the wind tunnel velocity reproduced the upward flow of velocity V_d on the rotor (Fig. 5). The rotor RPM was measured by a Hall switch installed on the rotor stand in conjunction with a magnet attached to the free spinning hub. A load cell between the rotor shaft and the rotor stand measured the rotor thrust. The rotor stand was designed to provide a stable support to the rotor/load cell assembly while at the same time minimizing any vibrations that could adversely affect the quality of the load cell measurement. The stand was also designed to minimize any flow disturbances. The free stream velocity V_d was measured using a Pitot probe connected to a pressure transducer. All data were acquired by a data acquisition computer running an in-house developed LabView based software. The test data were collected over a range of rotor parameters: blade pitch angle θ_o, pitch-flap coupling angle δ_3, blade precone angle β_p,

Table 1. Parameters of the scaled rotor model

Rotor diameter, m (inches)	0.33 (13)
Blade number, N_b	2
Blade span, m (inches)	0.1524 (6)
Blade chord, m (inches)	0.0287 (1.13)
Blade twist, deg/m (deg/inch)	0 (0)
Blade mass (g)	5.2
Airfoil	NACA 0010
Pitch angle (deg)	0, −6, −8, −12
Pitch-flap coupling angle, δ_3 (deg)	None; −17.33; −29.74
Precone angle, β_p (deg)	0 ; −4; −6

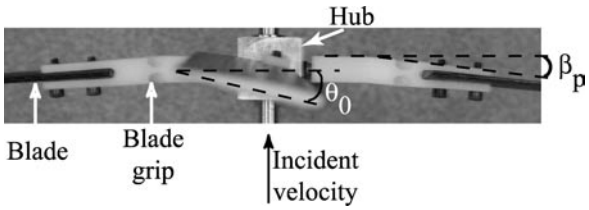

Fig. 3. Close-up view of the model rotor hub with the negative root pitch angle, θ_o, and the negative precone angle, β_p.

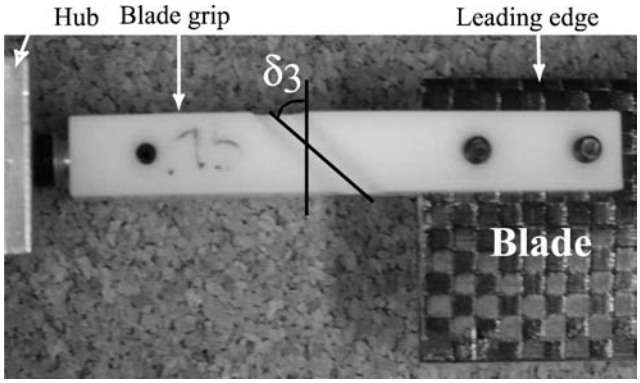

Fig. 4. Close-up view of the model rotor blade grip with the δ_3 hinge.

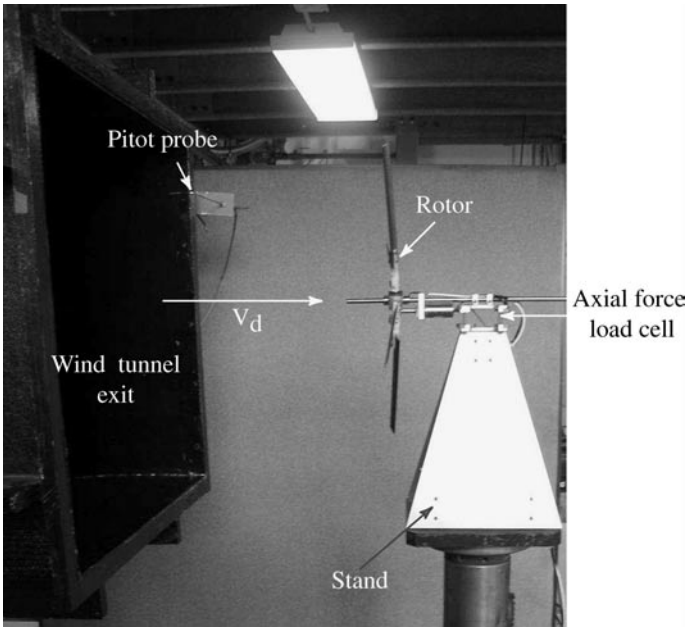

Fig. 5. Wind tunnel test setup.

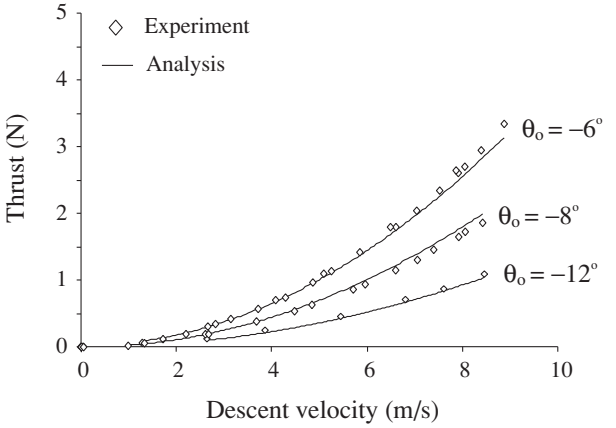

(a) Steady state thrust

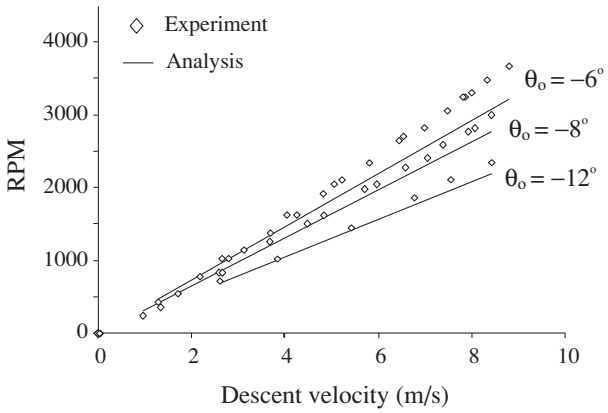

(b) Steady state RPM

Fig. 6. Analytical and experimental results from a 2-bladed rotor with stiff flap hinges, no pitch-flap coupling, precone $\beta_p = 0°$.

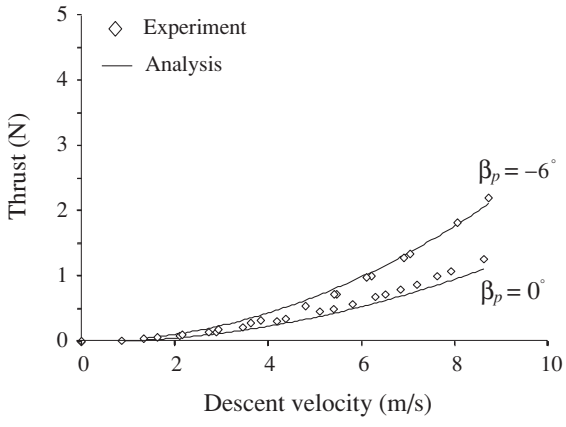

(a) Steady state thrust

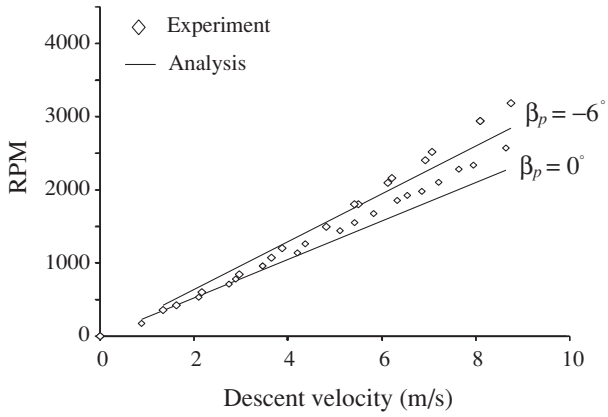

(b) Steady state RPM

Fig. 7. Analytical and experimental results from a 2-bladed rotor with a pitch-flap coupling $\delta_3 = -29.74°$ and pitch $\theta_o = -12°$.

and wind tunnel velocities V_d ranging from 1 to 9 m/s. The values of the tested pitch angles, δ_3 angles and precone angles are shown in Table 1.

Experimental Results

The measured steady state rotor thrust and RPM are plotted as a function of descent velocity V_d (wind tunnel velocity) in Figs. 6–8. The values of thrust and RPM calculated using the RPM sweep method are also plotted. From these figures, the effect of rotor parameters on the performance of the rotor, as well as the correlation of the measurements with analysis, can be evaluated.

Influence of rotor parameters

The influence of the design parameters on the performance of the rotor can be evaluated by comparing the steady thrust and RPM of the rotor at a specific descent velocity, while changing the rotor parameters between each test run, as indicated in Table 1.

Effect of blade pitch θ_o. The variation of steady state thrust and RPM as a function of descent velocity for blade pitch angles of $\theta_o = -6°, -8°$, and $-12°$ is shown in Fig. 6. For these tests, the rotor was configured with a rigid flap hinge as well as zero precone. At $V_d = 8$ m/s, the thrust decreases from 2.5 N to approximately 1 N and the RPM decreases from 3,400 to 2,200. It can be concluded that the thrust and RPM decrease with lower blade pitch. This is because a lower blade pitch effectively translates to a lower steady state angle of attack. The same trend is observed in other groups of tests that feature different values of precone angle and pitch-flap coupling, and is independent of the value of V_d.

Effect of precone β_p. Figure 7 shows the steady state rotor thrust and RPM as the precone angle decreases from $\beta_p = 0°$ to $\beta_p = -6°$. For these tests, the pitch-flap coupling angle was set at $\delta_3 = -29.74°$ and the blade pitch was $\theta_o = -12°$. For $V_d = 4.5$ m/s, the thrust increases from 0.35 to 0.54 N and the RPM increases from 1,440 to 1,500. It can be concluded that the thrust and RPM increase with more negative precone. Note that for the cases with the rigid flap hinge, the measured thrust and RPM are independent of the precone angle. This is because the main influence of decreasing the precone angle is to increase the effective change in flap angle at steady state. Therefore, the precone angle is not effective in the case of a rigid flap hinge.

Effect of pitch-flap coupling angle δ_3. Figure 8 shows the steady state rotor thrust and RPM as the pitch-flap coupling angle is changed from $\delta_3 = -29.74°$ to $\delta_3 = -17.33°$. The blade pitch was kept at $\theta_o = -12°$ and the precone was kept at $\beta_p = -6°$ for these tests. For $V_d = 6.5$ m/s, the thrust decreases from 0.99 to 0.85 N as the δ_3 angle is increased, and the RPM decreases from 2,160 to 2,100. Therefore the thrust and RPM increase with more negative pitch-flap coupling.

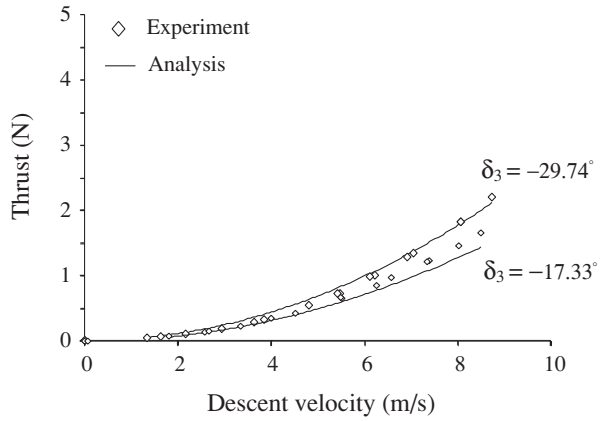

(a) Steady state thrust

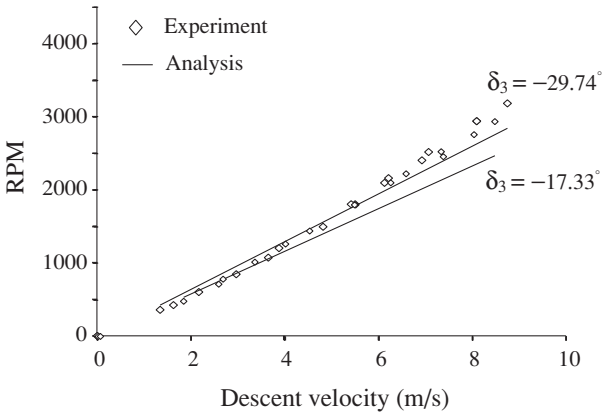

(b) Steady state RPM

Fig. 8. Analytical and experimental results from a 2-bladed rotor with a precone $\beta_p = -6^\circ$ and pitch $\theta_o = -12^\circ$.

Correlation with analysis

In order to compare the trends of the measurements, and to correlate the analysis with measured results, it is useful to represent the data in terms of a polynomial curve fit. From the experimental results, it was observed that the variation of thrust with wind velocity was quadratic and the variation of RPM with wind velocity was linear. For each plot of thrust versus V_d and RPM versus V_d, a curve can be fitted to the experimental data points. Similarly, the values of thrust and RPM calculated at each descent velocity using the RPM sweep method can be expressed in terms of polynomials. The measured thrust, T_{exp}, measured RPM, Ω_{exp}, analytical thrust, T_{ana} and analytical RPM, Ω_{ana}, are given by

$$T_{\text{exp}} = a_o^e V_d^2 \tag{9}$$

$$\Omega_{\text{exp}} = b^e V_d \tag{10}$$

$$T_{\text{ana}} = a_o^a V_d^2 \tag{11}$$

$$\Omega_{\text{ana}} = b^a V_d \tag{12}$$

where the superscript e refers to coefficients from measured data and the superscript a refers to coefficients from the analysis. Comparing the coefficients a_o^e with a_o^a and b^e with b^a provides a convenient means to evaluate the accuracy of the analytical predictions with respect to the experimental data. Table 2 shows the a_o^e, a_o^a, b^e and b^a coefficients for each test case. The error between the analysis and measured values is given in terms of the error in thrust, E_T, and the error in RPM, E_{RPM}.

In most cases the analysis underestimates the thrust and RPM. In general, the analysis shows the correct trends and around 10 to 15% magnitude error in both thrust and RPM. However, for some cases the correlation is less accurate, with errors of up to 25%. The errors do not appear to exhibit any definite trends with the test variables; however, in general the analysis is less accurate for the cases with $\delta_3 = -17.33^\circ$.

The discrepancy between the analysis and measurements can be attributed to two main causes. Firstly, the underlying physics impose

Table 2. General wind tunnel test matrix

Case No.	θ_o (deg)	δ_3 (deg)	β_p(deg)	a_o^e	a_o^a	E_T (%)	b^e	b^a	E_{RPM} (%)
1	−6	None	0	0.0427	0.0396	7.2	403.71	362.93	10.1
2	−8	None	0	0.0254	0.0279	−9.8	343.93	326.54	5.0
3	−12	None	0	0.0138	0.0141	−2.1	273.77	262.1	4.2
4	−6	−29.74	0	0.0452	0.0442	2.2	404.05	373.8	7.4
5	−8	−29.74	0	0.0372	0.0307	17.4	385.99	336.11	12.9
6	−12	−29.74	0	0.016	0.0149	6.8	290.45	263.55	9.2
7	−6	−29.74	−4	0.092	0.0708	23.04	459.8	354.1	22.9
8	−8	−29.74	−4	0.0688	0.0637	7.41	459.92	355.18	22.77
9	−12	−29.74	−4	0.0297	0.0225	24.2	352.84	302.48	14.2
10	−6	−29.74	−6	0.0833	0.0699	16.0	421.28	399.52	5.1
11	−8	−29.74	−6	0.0669	0.0561	16.1	415.04	393.86	5.1
12	−12	−29.74	−6	0.0333	0.0279	16.2	346.04	323.99	6.3
13	−6	−17.33	0	0.076	0.0581	23.5	446.8	344.02	23.0
14	−8	−17.33	0	0.0486	0.0505	3.9	423.5	327.19	22.74
15	−12	−17.33	0	0.0181	0.0146	19.3	309.96	261.35	15.6
16	−6	−17.33	−4	0.0808	0.0628	22.27	467.22	354.71	24.0
17	−8	−17.33	−4	0.0548	0.0557	1.6	420.08	336.66	19.8
18	−12	−17.33	−4	0.0227	0.0181	20.2	330.22	281.13	14.8
19	−6	−17.33	−6	0.089	0.0679	23.7	499.5	376.14	24.7
20	−8	−17.33	−6	0.0538	0.0413	23.2	437.05	366.17	16.2
21	−12	−17.33	−6	0.0242	0.0202	16.5	334.1	291.74	12.6

fundamental limits on the analysis. Autorotation occurs in the vortex ring state of the rotor where there is no well-defined slipstream. The flow behind the rotor is highly unsteady, and no analytical model appears to exist that can capture the behavior of the rotor in this state. The RPM sweep method represents an approximation to this physical condition, obtained by extrapolating the rotor torque versus RPM curve. As the curve reaches zero rotor torque (Fig. 2), the slope of the curve decreases and becomes close to zero. Consequently, it is difficult to obtain the exact point of intersection of the curve with the zero torque axis. This presents an additional approximation in the analysis. Second, the steady rotor thrust and RPM are extremely sensitive to the blade pitch angle. An error of even 1° in setting the blade pitch angle on the rotor model will result in a significant error in the predicted value of rotor thrust and RPM. It can be concluded that the error in the analysis is acceptable within the limits of the simplistic approach of the RPM sweep method, and the present analysis is satisfactory as a preliminary design tool.

It is interesting to investigate the sensitivity of the analysis to the choice of the airfoil profile drag coefficient. For instance, if $C_d = 0.02$ is used instead of $C_d = 0.04$ the calculated RPMs were closer to the measured data. For example, in case No. 19, for $C_d = 0.02$ the RPM error $E_{\text{RPM}} = 11\%$, whereas for $C_d = 0.04$ the RPM error is $E_{\text{RPM}} = 24.7\%$. However, using a lower C_d value increases the error in thrust predictions. For case No. 19, the thrust error $E_T = 23.7\%$ for $C_d = 0.04$, and in the case of $C_d = 0.02$, the thrust error is $E_T = 52.3\%$. Hence, the use of $C_d = 0.04$ in the analysis is justified.

Parametric study

The wind tunnel tests gave an understanding of the behavior of the system and of the influence of the initial collective pitch, pitch-flap coupling, and precone angles. Using the RPM sweep method, a parametric study is performed on the rotor design variables. The descent velocity is chosen as 4.57 m/s, and the variables of the parametric study are the blade pitch angle θ_o, pitch-flap coupling angle, δ_3, precone angle, β_p, and the blade mass m_b. The baseline case is chosen as 1) blade pitch, $\theta_o = -12^\circ$; 2) pitch-flap coupling angle, $\delta_3 = -17.33^\circ$; 3) precone angle, $\beta_p = -6^\circ$; and 4) blade mass $m_b = 0.0052$ kg.

The effect of the design variables is summarized in Figs. 9–12 and in Table 3. It can be seen that thrust and RPM vary monotonically with each design parameter, and no optimum value exists. The values for the full scale Autobody must take into account other mechanical considerations and are chosen as follows:

1) The value of blade pitch should be chosen as high as possible to maximize the thrust; however, the pitch at 3/4 radius should be negative to initiate rotation in the correct direction.

2) For δ_3 angles lower than -50°, the analysis showed that the blade gets stalled. Therefore, the optimum δ_3 value for the Autobody was chosen to be -45° to avoid stall and achieve a high steady state thrust.

3) An ideal value of precone would be as negative as possible. However, a large precone would result in a decrease in disk area and high stresses at the blade root. A value of -4° is chosen for the full-scale Autobody.

4) The lowest possible blade mass will result in the best performance. However, care must be taken to maintain an acceptable blade stiffness.

In addition, it should be noted that the quantitative influence of each parameter is different. Table 3 presents the variation in steady state thrust and RPM for a change of 100% in each parameter from the baseline values. It can be seen that the parameters with the greatest influence on rotational velocity and thrust are the δ_3 angle and the blade pitch. The precone and the blade mass have less influence on the thrust and RPM.

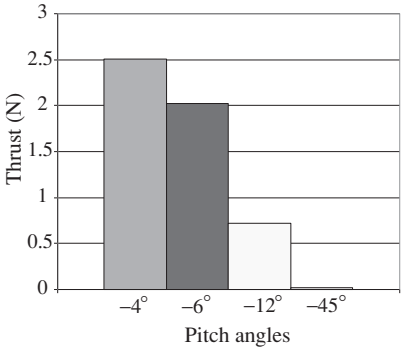

(a) Thrust

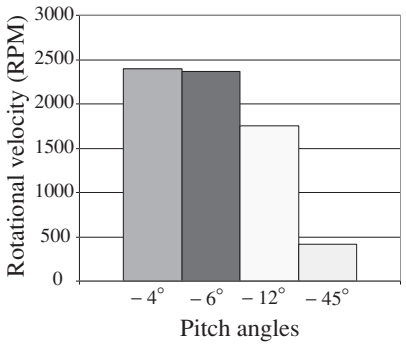

(b) RPM

Fig. 9. Thrust and rotational velocity for different pitch angles.

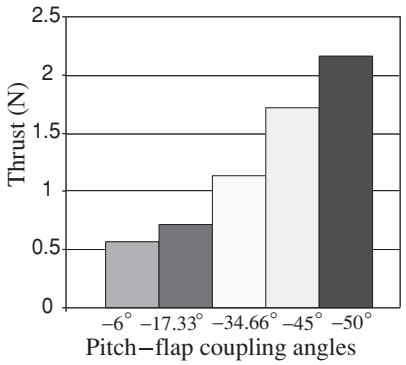

(a) Thrust

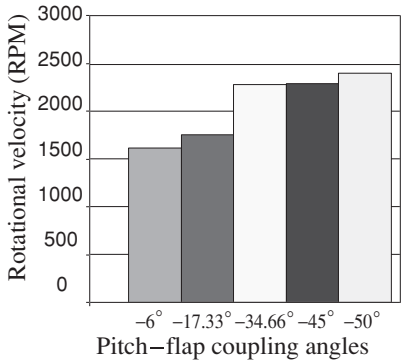

(b) RPM

Fig. 10. Thrust and rotational velocity for different pitch-flap coupling angles.

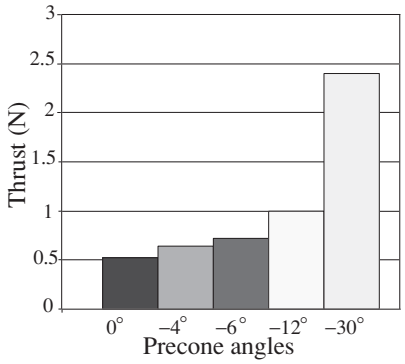

(a) Thrust

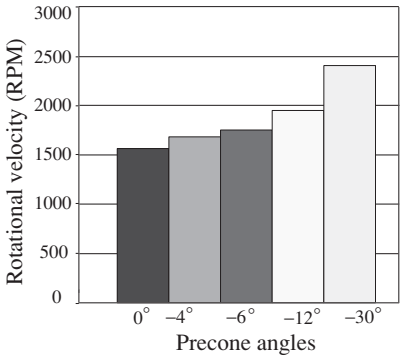

(b) RPM

Fig. 11. Thrust and rotational velocity for different precone angles.

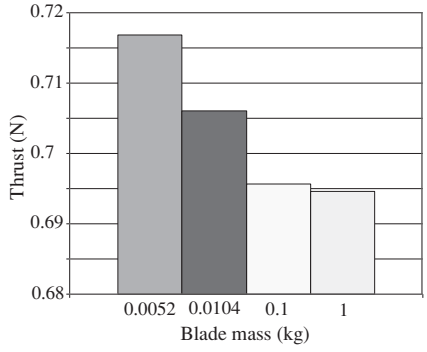

(a) Thrust

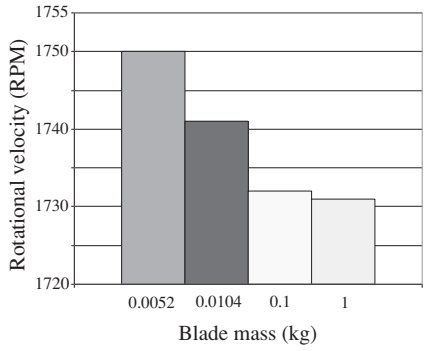

(b) RPM

Fig. 12. Thrust and rotational velocity for different blade masses.

Table 3. Sensitivity of steady state thrust and RPM on design parameters

Parameter	Parameter Variation (%)	Ω Variation (%)	T Variation (%)
θ_o	+100	−25	−63
δ_3	+100	+30.2	+58.3
β_p	+100	+11.7	+39
m_b	+100	−0.51	−1.5

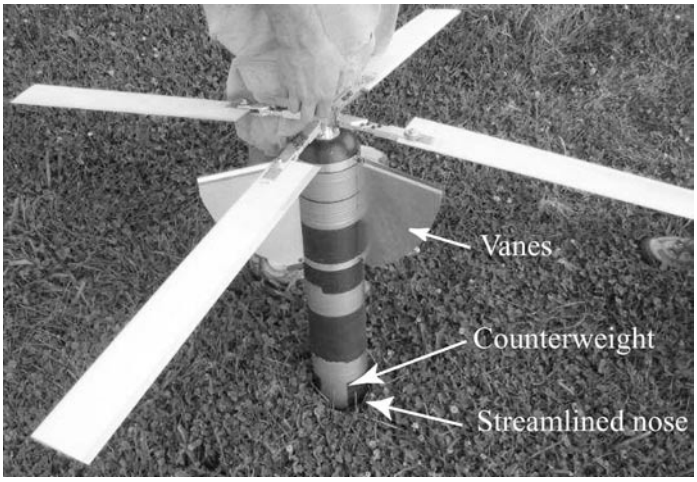

Fig. 13. Full-scale Autobody configuration.

Flight Tests

A full-scale prototype Autobody was designed based on the results of the parametric study, and was flight tested with on-board instrumentation to measure the descent velocity and the rotor RPM. The data were correlated with a modified version of the RPM sweep analysis.

Prototype construction

The full-scale prototype is shown in Fig. 13. The fuselage was a long cylindrical body of diameter 4 inches, terminated by a heavy round nose. The prototype incorporated a 48-inch diameter, four-bladed rotor attached to the body by means of a free spinning hub. The full-scale rotor was designed with an adjustable blade pitch, a negative precone $\beta_p = -4^\circ$, and a negative pitch-flap coupling angle $\delta_3 = -45^\circ$.

The blade grips of the full-scale rotor consist of two parts, linked by a clamped spring steel shim, which acts as a flexure and constitutes the δ_3 hinge (Fig. 14). The actual value of the δ_3 angle was measured to be -41° due to the finite width of the flexure. The flapping stiffness of the hinge could be changed by varying the thickness of the spring steel shim. A lag hinge was incorporated in the blade grip so that the rotor blades could rotate about this hinge to absorb the energy during landing impact. The blades were manufactured with a positive twist and a rectangular planform, and consisted of a foam core covered with two plies of IM7/8552 carbon fiber weave. Two sets of blades were manufactured, each with a different mass. The parameters of the full-scale rotor are summarized in the flight test matrix shown in Table 4.

The blades had a tip twist of $+7.75^\circ$ to achieve a more uniform distribution of angle of attack along the span of the blade. In order to initiate rotor rotation in the correct direction, the blade pitch at 3/4 span must be negative, i.e., $\theta_{0.75} < 0$. Therefore, the blade root pitch must meet the condition $\theta_o \leq -5.8^\circ$.

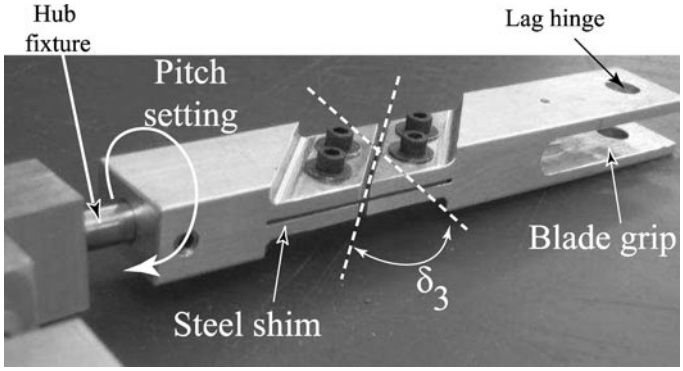

Fig. 14. Features of the full-scale rotor blade grip with a δ_3 of $-41°$.

Table 4. Flight tests matrix

Test Number	1	2	3
Rotor diameter, m (inches)	1.22 (48)	1.22 (48)	1.22 (48)
Number of blades, N_b	4	4	4
Blade span, m (inches)	0.508 (20)	0.508 (20)	0.508 (20)
Blade chord, m (inches)	0.0762 (3)	0.0762 (3)	0.0762 (3)
Blade airfoil	SC 1095	SC 1095	SC 1095
Blade tip twist, deg	+7.75	+7.75	+7.75
Root pitch angle, deg	−10	−9	−10
δ_3 angle, deg	−41	−41	−41
Precone angle, β_p, deg	−4	−4	−4
Blade mass, g	84.6	61.3	84.6
Flapping stiffness, k_β, Nm/rad	313	313	94

Instrumentation

On-board instrumentation was installed to acquire rotor RPM, acceleration along the rotor shaft axis and height data. The sensors are connected to an on-board micro-recorder, the Tattletale TT8V2, and the data were recorded as a function of time. The instrumentation consisted of 1) a Hall switch to measure RPM in conjunction with a magnet mounted on the rotor shaft; 2) an *ADXL*−202 two-axis accelerometer mounted in the Autobody such that one of the sensing directions is aligned with the longitudinal axis of the Autobody. The vertical acceleration is used to identify the steady state condition; and 3) a pressure transducer to measure the static pressure inside the body. The height can be obtained from these readings and is used to obtain the descent velocity.

Test matrix

Three different configurations were tested (Table 4) to determine which one achieved a rate of descent lower than 4.57 m/s. The full-scale configurations were tested by dropping them from a hot air balloon, released from altitudes of 305 (1,000 ft), 244 (800 ft), and 250 m (820 ft), respectively.

Flight test results

In each flight test, the vertical acceleration and rotor RPM data were recorded as a function of time and the steady state values were validated with the analysis. Based on the results of each test, the rotor parameters were changed appropriately in order to achieve the goal of steady state descent velocity less than 4.57 m/s.

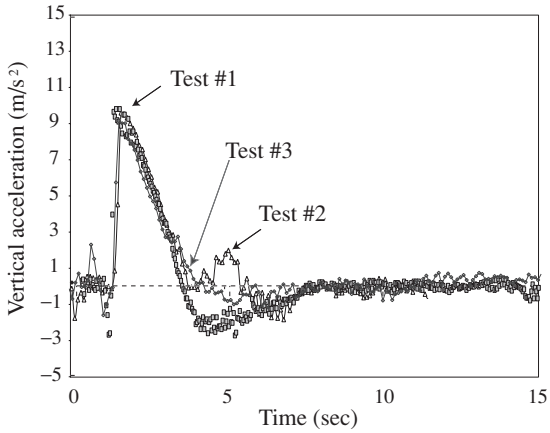

Fig. 15. Comparison of vertical acceleration data time history recorded during different flight tests.

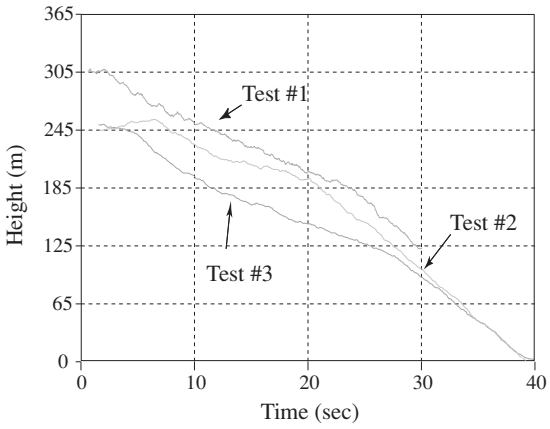

Fig. 16. Comparison of autobody height data time history recorded during different flight tests.

Figures 15–17 show the vertical acceleration, height, and rotor RPM as a function of time for the three flight tests. The transient as well as steady state response of the Autobody can be clearly seen from the vertical acceleration shown in Fig. 15. The Autobody was held in the balloon for 0.8 s and then released. During this time, the Autobody was stationary, and its vertical acceleration was zero. At this point, its height was constant and equal to the reference altitude of 305 m (Fig. 16). From Fig. 15, it can be seen that at the instant of release, the Autobody experiences an acceleration of 1 g. Thereafter, the rotor starts producing an increasing amount of thrust and decelerates the system. From 2.5 to 6.5 s from the release, the vertical acceleration becomes negative because the thrust produced by the rotor is greater than the weight of the vehicle. After approximately 6.7 s from the release, the vehicle stabilizes and enters the steady state of autorotation, characterized by zero vertical acceleration.

It was observed that after approximately 13 s, the Autobody started precessing. This can be seen as an oscillation in the vertical acceleration and RPM (Fig. 15 and 17) values. Because of the precession, the thrust decreased and the rate of descent increased, as seen in Fig. 16. The precession was caused due to small dissimilarities between the blades, such as differences in mass due to the manufacturing process, and differences in setting the blade pitch angle. Elimination of the precession will involve tracking the rotor before launch, and will be an important practical design consideration in terms of the final application of the Autobody.

Figure 17 shows the rotor RPM as a function of time. Because of a data capture error, the RPM data could not be acquired during the third drop test. However, the value of the steady state RPM for the first two drop tests can be extracted from the recorded data.

It can be seen that the height obtained from the pressure transducer has a significant noise level (±6 m (≈20 ft)). Therefore, the descent velocity was obtained by first calculating a moving average of the height data, and then performing a numerical differentiation. Note that as the sampling rate of the on-board datalogger was limited, it was not possible to obtain the descent velocity by integration of the acceleration data.

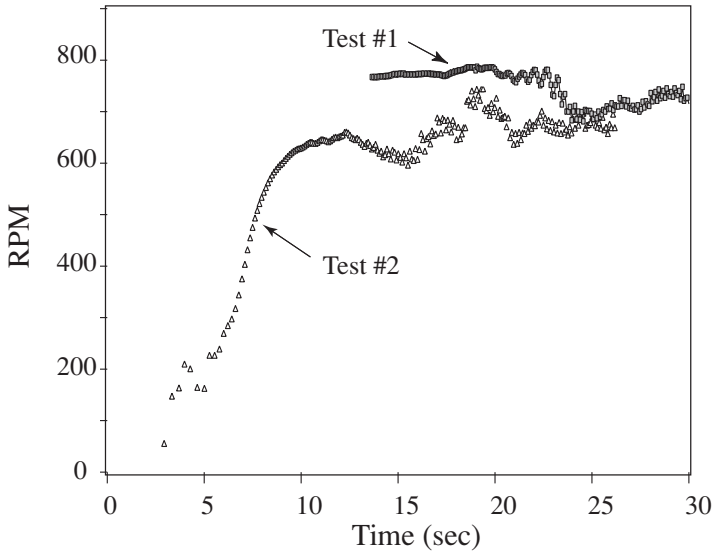

Fig. 17. Comparison of rotor RPM data time history recorded during different flight tests.

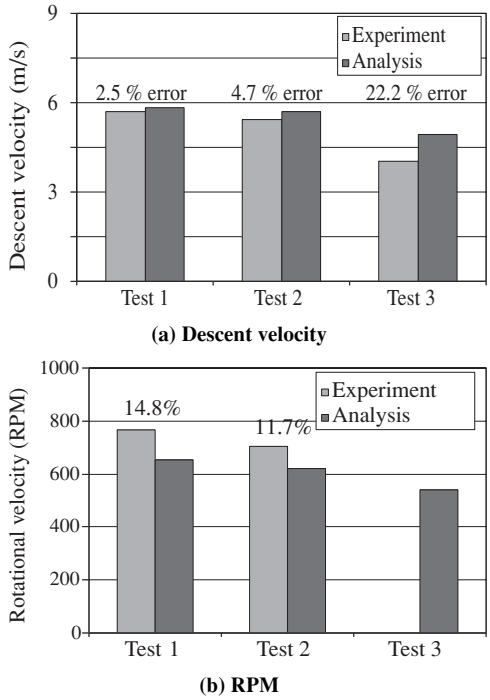

Fig. 18. Correlation of steady state descent velocity and rotor RPM data with analytical predictions for the three flight tests.

Correlation with analysis

Analytical results are compared with data measured during the three flights in Fig. 18. The analysis shows good agreement with the measured descent velocity. The maximum error between analysis and experiment is 22.2% and occurs in the third flight test. Note that the third test was performed with the lowest flapping stiffness k_β and it is expected that the dissimilarities between the k_β of the blades had a larger effect. The measured descent velocity for the third test is 4.11 m/s (13.5 ft/s). Therefore, this Autobody design meets the requirement of a descent velocity lower than 4.57 m/s. The measured RPM also shows good agreement with the analysis, with a maximum error of less than 15%.

Summary and Conclusions

Analytical and experimental studies have been carried out to investigate the behavior of an autonomous vehicle with passive controls, called the Autobody. It is designed to passively deploy a payload from an aircraft by means of an autorotative rotor, with a steady state descent velocity of less than 4.57 m/s. Only purely vertical autorotation is considered as it results in a conservative design, and presents the simplest case for analysis.

A negative blade pitch was incorporated to start the rotor rotation in the correct direction (i.e., leading edge first). A novel mechanism consisting of a negative pitch-flap coupling in conjunction with a negative precone was incorporated to passively increase the pitch of the rotor blades as the rotational speed increased. These concepts ensured that the rotor rotation was initiated in the correct direction and that enough steady state thrust was generated to minimize the descent velocity of the system.

An analytical study, called the RPM sweep method, based on blade element momentum theory, was developed to predict the behavior of the Autobody in steady state of autorotation. The method consists of sweeping through a range of RPMs such that the rotor remains in the windmill brake state, and calculating the thrust and torque of the rotor at each RPM. The torque versus RPM curve is extrapolated to the zero torque point, which indicates the RPM at which autorotation occurs.

Wind tunnel tests were performed on a scaled model rotor to establish the proof-of-concept of the rotor design, to investigate the influence of the rotor design parameters on the steady state performance of the rotor and to validate the analysis. The thrust and RPM were measured for several values of wind velocities V_d, blade pitch, pitch-flap coupling, and precone angles. It was observed that variation of thrust with V_d was quadratic and the variation of RPM with V_d was linear. Furthermore, it was observed that the experimental data and analytical predictions show good agreement with a maximum error of around 25%.

A parametric study was carried out to investigate the influence of blade pitch, pitch-flap coupling angle, precone angle, and blade mass on the steady state thrust and RPM. Based on this quantitative parametric study and on mechanical considerations, an optimum full-scale configuration was determined to achieve the objective of steady state descending velocity less than 4.57 m/s. Instrumented flight tests on this configuration were conducted to obtain rotor RPM, vertical acceleration, descending velocity and altitude of the Autobody during the transient and steady states of autorotation. The Autobody was dropped from a hot air balloon and the data were recorded on an on-board microrecorder. It was observed that a steady state rate of descent of 4.11 m/s was attained for a rotor with a blade pitch angle $\theta_o = -10^\circ$, a pitch-flap coupling angle $\delta_3 = -41^\circ$, and a precone angle $\beta_p = -4^\circ$ and having blades of mass $m_b = 85.4$ g each. This configuration met all the requirements and is therefore a successful design. Furthermore, the full-scale flight test experimental results showed good agreement with the analytical predictions. The maximum error between analysis and experiment was 22.2%

for the prediction of the descending velocity during one of the flight tests.

An analysis of the transient state of the flight should be developed to describe more accurately the behavior of the Autobody during its flight. Improvements must also be carried out in the design and manufacturing of the δ_3 hinge. Repeatable and precise manufacturing process of the flexure hinge would ensure that all the hinges have equal flapping stiffness and therefore allow each blade to flap and pitch in a similar fashion. This would assure a tracked rotor and stable flight without precession. Finally, more reliable instrumentation should be used to perform further flight tests. Specifically, a higher sampling rate microrecorder should be used and means of measuring height and descending velocity more accurately should be developed.

Acknowledgments

The authors acknowledge Mr. Seibert Murphy from Progeny Systems who provided the initial impetus for this research. We thank Dr. Marat Tishchenko for his help and advice, Dr. V. T. Nagaraj for his advice, and Mr. Nitin Gupta for his help in the experimental testing.

References

[1]Hudson, G. C., "Roton Development and Flight Test Program," AIAA-1998-5258, AIAA Defense and Civil Space Programs Conference and Exhibit Proceedings, Huntsville, AL, October 28–30, 1998.

[2]Leishman, J. G., *Principles of Helicopter Aerodynamics*, Cambridge University Press, New York, 2000.

[3]Leishman, J. G., "The Autogyro: The First Rotating-Wing Aircraft. Part 1 : That Curious Phenomenon of Autorotation," *Vertiflite*, Vol. 49, (2), 2003, p. 48.

[4]Prouty, R. W., *Helicopter Performance, Stability, and Control*, Krieger Publishing Company, Malabar, FL, 2002.

[5]Prouty, R. W., "Torque Distribution in Autorotation," *Vertiflite*, 48, (2), 2002, p. 28.

[6]Lambermont, P., and Pirie, A., *Helicopters and Autogyros of the World*, Cassell, London, 1958.

[7]Bartz, J., and Miklosovic, D. S., "An Experimental Analysis of Camber Effects of a 6-Bladed Flapped Autorotational Aerodynamic Decelerator," AIAA-2003-2143, 17th AIAA Aerodynamic Decelerator Systems Technology Conference and Seminar, Monterey, CA, May 19–22, 2003.

[8]Wernicke, R. F., "Preliminary Tests of Model Spacecraft Rotor Landing System," Technical Report, Bell Helicopter Corporation, Fort Worth, TX, 1959.

[9]Kretz, M., "Space Rotor—A European Project for Recovery of Heavy Launch Vehicles (Reentry and Recovery of Space Vehicles in Reliable Shock Free Landings, Using Modified Helicopter Rotor for Hypersonic Flow and Thermal Problems)," *Spaceflight*, Vol. 8, 1966, pp. 369–373.

[10]Levin, A. D., and Smith, R. C., "An Analytical Investigation of the Aerodynamic and Performance Characteristics of an Unpowered Rotor Entry Vehicle," Technical Report, NASA TN D-4537, April 1968.

[11]Levin, A. D., and Smith, R.C., "Experimental Aerodynamics of a Rotor Entry Vehicle," *Journal of Aircraft*, Vol. 6, (4), 1969, pp. 330–335.

[12]Sirohi, J., Nagaraj, V. T., and Chopra, I., "Design and Testing of a Rotor for Autonomous Autorotation," American Helicopter Society 60th Annual Forum Proceedings, Baltimore, MD, June 7–10, 2004.

[13]Castles, W., Jr., and Gray, R. B., "Empirical Relation between Induced Velocity, Thrust, and Rate of Descent of a Helicopter Rotor as Determined by Wind-Tunnel Tests on Four Model Rotors," NACA TN-2474, 1951.